

Isotope-shift and hyperfine-constant measurements of near-infrared xenon transitions in glow discharges and on a metastable Xe(3P_2) beam

G. D'Amico, G. Pesce, and A. Sasso

Dipartimento di Scienze Fisiche, Università "Federico II" di Napoli and INFN, Complesso Universitario Monte S. Angelo, Via Cinthia, 80125 Napoli, Italy

(Received 19 April 1999)

In this paper we discuss the hyperfine structure and isotope shift of the xenon atom. The study was performed using a semiconductor diode laser mounted in an extended-cavity configuration and emitting in the near-infrared range of spectrum. Doppler-free spectra of four transitions between 820 and 830 nm were obtained by using either a saturation spectroscopy technique in a cell or a laser-induced fluorescence technique on a collimated atomic metastable beam. The hyperfine coupling constants of ^{129}Xe and ^{131}Xe were determined for the levels $1s_5$, $1s_4$, $1s_2$, $2p_2$, $2p_4$, and $2p_6$ (Paschen notation). Moreover, a systematic study of the isotope shift was performed for the $1s_3 \rightarrow 2p_4$ ($\lambda = 820.8$ nm) and $1s_5 \rightarrow 2p_6$ ($\lambda = 823.3$ nm) transitions for which all the stable isotopes $^{128-131}\text{Xe}$, ^{132}Xe , ^{134}Xe , and ^{136}Xe were fully resolved. [S1050-2947(99)02712-2]

PACS number(s): 32.30.Jc

I. INTRODUCTION

Accurate measurements of isotope shift (IS) and hyperfine structure (HFS) in atoms allow us to obtain precious information about the coupling of the nucleus with its electronic environment and thus to test quantum-mechanical calculations based on Hartree-Fock methods. In particular, the investigation of nuclear effects on the optical electrons allows us to estimate changes in mean-square radii from isotope to isotope, nuclear deformations, nuclear magnetic-dipole and electric-quadrupole interaction constants. Alternatively, if nuclear parameters are available they can provide information about electronic properties, such as screening factors or electronic correlation effects.

The spectra of rare-gas atoms are characterized by $ns-np$ series in the visible and near-infrared spectral regions. These transitions connect the metastable 3P_0 and 3P_2 states and the radiative 3P_1 and 1P_1 states with energetically higher levels. On the other hand, the transitions starting from the ground state 1S_0 are in the vacuum ultraviolet range where tunable laser sources of high spectral purity are not yet available.

The xenon atom ($Z=54$) is of particular interest for a systematic study of IS and HFS because it has nine stable isotopes in natural abundance accessible to high sensitivity laser spectroscopy techniques ($^{124}\text{Xe}:0.0096\%$, $^{126}\text{Xe}:0.0090\%$, $^{128}\text{Xe}:1.92\%$, $^{129}\text{Xe}:26.4\%$, $^{130}\text{Xe}:4.1\%$, $^{131}\text{Xe}:21.1\%$, $^{132}\text{Xe}:26.9\%$, $^{134}\text{Xe}:10.4\%$ and $^{136}\text{Xe}:8.9\%$). In addition, two of these nuclei have a nuclear spin ($^{129}\text{Xe}:I=\frac{1}{2}$ and $^{131}\text{Xe}:I=\frac{3}{2}$) which brings about a hyperfine splitting of the levels. Finally, this series of Xe isotopes crosses the closed neutron shell $N=82$ (^{136}Xe is a magic nucleus) and this can result in interesting anomalies in the IS.

Isotope shifts and hyperfine structure in xenon have been measured in many transitions by using different experimental approaches. Jackson and co-workers have measured the isotope shifts [1-3] and the hyperfine structure splittings [4,5] in isotopically enriched samples for a wide variety of transitions in the visible and near-infrared spectral regions by us-

ing classical interferometry with a full width at half maximum around 1 GHz. In particular, in Ref. [3] they provide an interpretation of the IS based on a parametric model and obtain reasonable agreement with *ab initio* Hartree-Fock calculations. Similar interferometric analysis of IS and HFS was also performed by Fischer *et al.* in Ref. [6].

Very precise determinations of the hyperfine splittings of the metastable 3P_2 state were achieved by Faust and Dermott [7] by using the atomic beam nuclear magnetic resonance method (NMR).

High-resolution studies of optical IS and HFS have been facilitated by well consolidated Doppler-free laser spectroscopy techniques and by the use of atomic beam technology. The IS and HFS constants of many xenon isotopes far from stability were investigated for the $6s\ 3/2\ [3/2]_2 \rightarrow 6p\ 3/2\ [3/2]_2$ (pair coupling notation: $nI\ J_{\text{core}}[K=J_{\text{core}}+1]_j$) transition ($\lambda = 823.3$ nm) by collisional ionization laser spectroscopy [8] at the ISOLDE facility at CERN.

Geisen *et al.* [9] investigated the transitions $6s\ 1/2\ [1/2]_0 \rightarrow 8p\ 1/2\ [1/2]_1$ ($\lambda = 626.5$ nm) and $6s\ 3/2\ [3/2]_2 \rightarrow 5d\ 3/2\ [P]_3$ (650.7 nm) by means of the laser-induced fluorescence technique on a beam of metastable Xe(3P_2) and Xe(1P_1) atoms.

Doppler-free two-photon laser spectroscopy was used by Plimmer *et al.* [10] in order to investigate the IS in two-photon transition at 249 nm from the $5p\ 6\ ^1S_0$ ground state to a $J=0$ level of the $5p\ 5\ 6p$ configuration (the $2p_5$ level in Paschen notation) for which the HFS was absent at both levels.

The development of laser cooling and trapping techniques has recently [11] allowed precise IS measurements on cold atoms of the $6s\ 3/2\ [3/2]_2 \rightarrow 6p\ 3/2\ [5/2]_3$ transition ($\lambda = 882.2$ nm) by using a titanium:sapphire laser.

The advent of semiconductor diode lasers has made it easier to extend Doppler-free laser investigations in the near-infrared spectral region. In particular, saturated absorption spectroscopy of Xe has been performed recently by Beverini *et al.* [12] by using a diode laser emitting at 830 nm. However, the aim of that paper was mainly to demonstrate the use

TABLE I. Transitions investigated in this work.

Transition			
Pair coupling	Paschen	λ (Å)	$A_{ki}(10^{-6} \text{ s}^{-1})$ (Ref. [14])
$6s \ 3/2 [3/2]_2 \rightarrow 6p \ 3/2 [3/2]_2$	$1s_5 \rightarrow 2p_6$	8233.893	23
$6s \ 1/2 [1/2]_0 \rightarrow 6p \ 1/2 [3/2]_1$	$1s_3 \rightarrow 2p_4$	8208.593	9
$6s \ 1/2 [1/2]_1 \rightarrow 6p \ 1/2 [1/2]_1$	$1s_2 \rightarrow 2p_2$	8268.786	9
$6s \ 3/2 [3/2]_1 \rightarrow 6p \ 3/2 [1/2]_0$	$1s_4 \rightarrow 2p_5$	8282.389	33

of near-infrared diode lasers for the Doppler-free technique since their laser operated within a broadband regime and no laser frequency calibration was employed.

In our work we have used a diode laser for Doppler-free spectroscopic measurements of four transitions between 820 and 830 nm for the first time listed in Table I (for the sake of simplicity Paschen notation is also introduced and will be used throughout the present paper). In light of the work of Ref. [12] the spectral purity of our laser was increased by using an optical feedback stabilization technique; the laser bandwidth was reduced below 1 MHz, i.e., to a value smaller than the homogeneous width of the investigated lines. Doppler-free resolution was achieved by using either saturation spectroscopy in the cell or laser-induced fluorescence (LIF) on a collimated metastable xenon beam, depending on the particular investigated transition as will be explained in the next section. That allowed us to measure the HFS splittings for all the investigated lines and their relative nuclear magnetic dipole and electric quadrupole coupling constants with an accuracy less than 1 MHz. In particular, for the $1s_4$, $1s_2$, $2p_2$, and $2p_4$ levels these are the first data obtained on the basis of Doppler-free techniques, to the best of our knowledge.

In addition, a complete analysis of the IS was done for the transitions $1s_5 \rightarrow 2p_6$ and $1s_3 \rightarrow 2p_4$ for which the even isotopes were fully resolved. Combining our optical IS measurements with the nuclear charge radii available from muonic transitions it was possible to obtain the specific mass shift and the field shift contributions. Finally, using the semi-empirical Goudsmit-Fermi-Segrè formula we estimated the screening factors β for the $1s_3$ and $1s_5$ levels.

II. EXPERIMENTAL METHODS

The laser source used in this experiment was an extended cavity semiconductor diode laser (AlGaAs/GaAs, Sharp model LT015MD0) emitting at $\lambda = 826$ nm at room temperature. Typical output power was about 4 mW with an injection current of 100 mA, while the laser bandwidth was found to be several tens of MHz. A narrower bandwidth less than 1 MHz was achieved instead by using a frequency stabilization scheme based on optical feedback [13]. The diode was placed inside a pseudocavity consisting of a 1200 lines/mm diffraction grating mounted in Littrow configuration. The first-order diffracted beam was fed back into the diode cavity whose output facet had a reduced reflectivity. A 30% reflectivity beam splitter was placed between the laser and the grating in order to extract the two laser beams used in the experiment.

Coarse wavelength tuning was obtained by changing the

diode temperature by means of a thermoelectric cooler, while fine and fast tuning was achieved by varying the injection current. Frequency scans of about 3 GHz were accomplished by changing the injection current and the cavity length synchronously, the latter by moving the grating by means of a piezoelectric crystal (PZT).

To avoid undesirable optical feedback interfering with the laser, an optical isolator was inserted between the laser and the rest of the experimental setup.

The laser wavelength was measured with a traveling Michelson interferometer with an accuracy of one part in 10^7 while the frequency scans were calibrated by using the markers from a 1500 MHz (Coherent Model 240) and 300.5(1) MHz (homemade) free-spectral range (FSR) confocal Fabry-Perot (FP) interferometers. The first (FP) interferometer was essentially used to check the laser mode quality while the transmission peaks of the second one were recorded simultaneously to the investigated spectra for frequency calibration. The homemade FP interferometer was made out of quartz tube and its free-spectral range was determined by introducing on the laser beam sidebands with an electro-optic modulator. The fluctuations of the free-spectral range observed over a period of a few hours were of the order of 100 kHz.

Moreover, particular care was put in the calibration of the laser frequency. Indeed, especially for diode laser sources, the frequency scan was not perfectly linear due to the piezocrystal of the extended cavity. This was taken into account by recording the FP peaks and using a fit procedure where the nonlinear frequency behavior versus the free-spectral range steps was assumed by a quadratic function. The found best fit parameters were then used to convert the recorded x axis (pixels) into the linear frequency axis (MHz).

In order to study the IS and HFS in Xe we used two different experimental techniques depending on the transition being investigated. In particular, the transitions starting from the metastable 3P_0 and 3P_2 states were, in principle, suitable to be investigated with higher resolution by means of an atomic beam where perturbations due to collisions and discharge electric fields are practically eliminated.

A metastable beam was produced by striking a 0.4 A dc discharge directly through a gas jet coming from a nozzle 1 mm in diameter (see Fig. 1). The beam was collimated with a rectangular 1 mm \times 5 mm aperture placed downstream from the excitation region. The spot of the laser beam, approximately circularized by means of a pair of anamorphic prisms ($\Phi \approx 2$ mm), crossed the atomic beam perpendicularly at a distance of 40 cm from the excitation region. The laser beam was then re-reflected so that it crossed again the

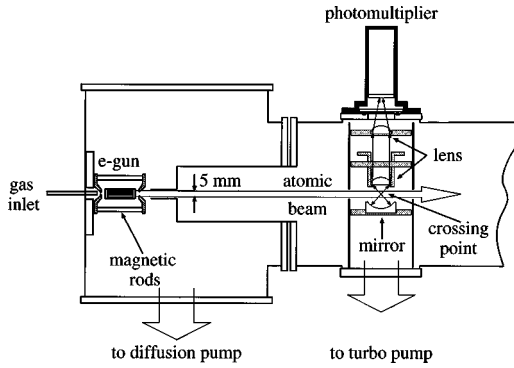


FIG. 1. Scheme of the experimental setup concerning the atomic metastable beam production and the interaction region with the laser beam.

beam in order to increase the fluorescence signal. Resonant fluorescence light from the crossing region was collected with an optical system consisting of a spherical mirror (5 cm in focal length) and a convergent lens of the same focal length; the crossing point was in the focal plane of both mirror and lens (see Fig. 1). Fluorescence photons were detected by a photomultiplier (Thorn EMI model 9203QB) while the scattered light was essentially suppressed by placing shields along the laser beam path.

We investigated transitions arising from both $1s_5$ and $1s_3$ metastable levels. Nevertheless, the fluorescence signal of the $1s_3 \rightarrow 2p_4$ transition resulted in about three orders of magnitude smaller than that of the $1s_5 \rightarrow 2p_6$ line. This result is apparently strange because the intensities of the two lines are comparable, as shown in Table I. However, the lifetimes of the two metastable levels are rather different, namely $\tau_{1s_5} = 150$ s and $\tau_{1s_3} = 80$ ms [14]. This difference is negligible with respect to the time of flight that metastable atoms take to reach the crossing region ($\tau_{\text{TOF}} \approx 1$ ms), but it plays a crucial role in the metastable production mechanisms. If we consider a simple rate equations model, the steady-state metastable densities n_3 and n_5 can be written as

$$n_{3,5} = \frac{n_e \sigma_{3,5} N_0}{1/\tau_{3,5} + K_{3,5}}, \quad (1)$$

where n_e is the electron density in the excitation region, $\sigma_{3,5}$ are the electron impact cross sections, and $K_{3,5}$ are the quenching rates for the two metastable levels. Since it is reasonable to consider $\sigma_3 \approx \sigma_5$ [15] and, as a first approximation, to neglect the role of collisional quenching in the expansion region of the atomic beam ($K_{3,5} = 0$), we have $n_5/n_3 \approx \tau_5/\tau_3 = 1875$, a figure whose order of magnitude is in agreement with the observed ratio.

Since the signal-to-noise ratio for the $1s_3 \rightarrow 2p_4$ line was too poor, this line was then investigated in a cell where atoms were excited by means of a radio-frequency discharge that has already been shown to be a very efficient system for the metastable production of noble gases [16].

The experimental setup for saturation spectroscopy is briefly described in the following: The laser beam was split into pump and probe beams with a power of 1 and 0.15 mW, respectively. The counter-propagating beams were weakly focused onto the discharge cell with 500 mm focal length

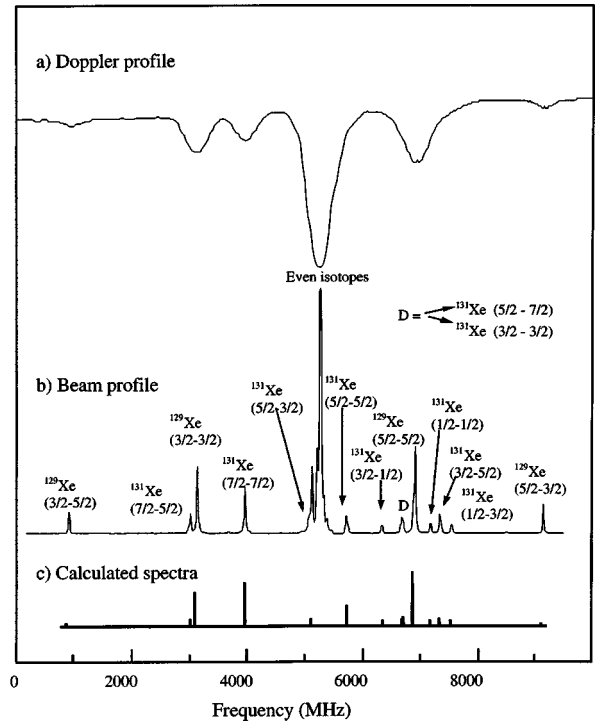


FIG. 2. Doppler-limited and Doppler-free spectra of the $1s_5 \rightarrow 2p_6$ transition: (a) represents the pure absorption signal recorded in the cell; (b) is the fluorescence signal on the atomic beam; (c) are the expected hyperfine patterns of ^{129}Xe and ^{131}Xe .

lenses. As a modulation system we used an acousto-optic modulator (AOM) instead of a mechanical chopper to increase the modulation frequency (thus reducing the $1/f$ noise of the laser) and to eliminate acoustic noise introduced by the mechanical chopper on the diode laser. The AOM deflected the laser beam at a frequency of 50 kHz while the laser frequency was swept at frequencies of a few Hz. The AOM also introduces a frequency shift of 20 MHz, although the saturation dip was not produced at the center of the investigated line this was trivial for isotope shift measurements. The analysis beam was detected by means of a fast photodiode and the electrical signal was amplified and phase sensitively rectified by a lock-in amplifier (integration time = 1 ms).

III. RESULTS AND DISCUSSION

A. Hyperfine structure

Figure 2(a) shows a typical Doppler-limited absorption spectrum for the $1s_5 \rightarrow 2p_6$ transition; the recording was obtained in a cell at a pressure of 0.5 Torr. As can be seen, the Doppler broadening ($\Delta \nu_D \approx 500$ MHz) masks completely the HFS which, for the transition being considered, should give place to 14 HFS components as well as the five peaks of the even isotopes.

A Doppler-free recording of the same transition obtained on an atomic beam with the LIF technique is reported in Fig. 2(b). The expected natural linewidth of this transition is 3.9 MHz while the observed width was about 10 MHz. This discrepancy can be ascribed to the residual Doppler broadening due to the collimation degree of our atomic beam since time-of-flight broadening and saturation broadening were

TABLE II. HFS coupling constants of ^{129}Xe and ^{131}Xe (in MHz). The uncertainties are one standard error obtained over a set of 20 recordings.

Level	HFS constant	Present work	Ref. [2]	Other measurements
$1s_5$	A^{129}	-2384.4(1.2)	2386(1.5)	-2384.5031(4) ^a , 2384(1.5) ^b
	A^{131}	705.4(4)		706.4747(7) ^a
	B^{131}	255.7(6)		252.5253(6) ^a , 252(2) ^b
$1s_4$	A^{129}	-959.1(7)	-971(3)	
	A^{131}	284.3(6)	287(9)	
	B^{131}	89.9(8)	87(9)	
$1s_2$	A^{129}	-5808(2)	-5806(4)	-5799(9) ^c
	A^{131}	1709.3(7)	1710(6)	1716(3) ^c
	B^{131}	30.3(8)	16(3)	24(6) ^c
$2p_2$	A^{129}	1977(1)	1979(4)	
	A^{131}	-581.0(6)	-583(6)	
	B^{131}	-6.2(4)	-5(6)	
$2p_4$	A^{129}	-4424(1)	-4427(3)	-4434(9) ^c
	A^{131}	-1321.8(9)	-1321(6)	-1314(9) ^c
	B^{131}	16.5(5)	16(3)	15(9) ^c
$2p_6$	A^{129}	-889.6(4)	-893(6)	-888(3) ^c , -886.1(8) ^d
	A^{131}	262.7(4)		263.1(6) ^d
	B^{131}	23.8(4)		29(2) ^d

^aReference [7].

^bReference [9].

^cReference [6].

^dReference [8].

negligible in our experimental conditions.

As can be seen from Fig. 2(b), the HFS pattern is spread over a relatively large frequency range (about 10 GHz). Since the maximum frequency scan of our laser system was only 3 GHz the spectra of Fig. 2(b) were obtained through five separate narrower scans so that at least one common line in each consecutive scanning was present. A similar procedure was followed for the other lines investigated in this work except the $1s_4 \rightarrow 2p_5$ line whose spectrum was recorded with a single frequency scanning.

The individual hyperfine components were identified on the basis of isotopic abundance, the intensity formulas for HFS multiplets [17] (see lower part in Fig. 2) and, where previous spectroscopic data were available, expected splitting patterns.

The spectrum of the $1s_3 \rightarrow 2p_4$ transition was a simpler matter because the lower level does not exhibit HFS ($J=0$), making an estimation of the hyperfine splittings easier. Experimental spectra were fitted using Lorentzian profiles for each peak taking as free parameters their centers, intensities, and widths (the latter was the same for all peaks). Some of the hyperfine splittings were determined from the separation of different couples of HFS components. In such cases we invariably found statistically consistent values and calculated the average among them to give the final result.

From the measured splittings the magnetic dipole (A) and electric quadrupole (B) coupling hyperfine constants were determined. In particular, for ^{129}Xe the constant A was calculated from the simple interval rule $\Delta_{(F,F-1)} = AF$ for $B=0$ ($I < 1$). For ^{131}Xe the constants A and B were obtained by fitting the hyperfine splittings to the well-known formula:

$$\Delta E_{(F,F-1)} = AF + \frac{3}{2}BF \left(\frac{F^2 + \frac{1}{2} - J(J+1) - I(I+1)}{IJ(2J-1)(2I-1)} \right). \quad (2)$$

The A and B constants measured in this work are listed in Table II and, where possible, they are compared with previous measurements reported in the literature. It is interesting to note that our measurements for the $1s_5$ level are in reasonable agreement with the very accurate NMR data. The agreement with the results previously obtained using laser techniques (see Ref. [8]) for the $2p_6$ level is also pleasing while some discrepancies are present with respect to the Doppler-limited interferometric data reported in Refs. [2] and [6]. Moreover, it is worth noting the rather small A constant for the $1s_4$ level in comparison to the A value of all other states of the $5p^5 6s$ electronic configuration.

The ratio between the magnetic dipole constants A for ^{129}Xe and ^{131}Xe should scale as the ratio of their nuclear moments ($\mu_{129} = 0.7768\mu_B$ and $\mu_{131} = 0.6908\mu_B$) and nuclear spins, and be equal to -0.2964 . The data of Table II are in agreement with this value for all the investigated levels within 1%. However, since hyperfine anomalies are expected to be $\ll 1\%$ the accuracy of our measurements is too poor to explore so fine an effect.

Another way to check the accuracy of our measurements is the estimation of the nuclear electric moment quadrupole Q from the measured B constant. As is well known these quantities are connected by the relation

$$B = -Q \left\langle \frac{\partial^2 V_e}{\partial z^2} \right\rangle$$

$$= -QC_e = -Q \left\langle J, m_J = J \left| \frac{3 \cos^2 \theta - 1}{r^3} \right| J, m_J = J \right\rangle, \quad (3)$$

where C_e is the mean gradient of the electric field generated by the electrons at the nucleus which can be easily calculated for an ls electronic configuration, with $l=p, d$ (for xenon the configuration $5p^5 6s$ gives place to four terms: $^3L_{l+1}$, 3L_l , $^3L_{l-1}$, and 1L_1). In this case it is possible to relate the quantities C_e with relativistic corrections and energy-level separations between the terms of the electronic configuration as described in more detail in Ref. [17]. These calculations lead to the following values of C_e :

$$C_e(^3P_2) = 8.99820, \quad C_e(^3P_1) = 3.30269,$$

$$C_e(^3P_0) = 0, \quad C_e(^1P_1) = 2.32124. \quad (4)$$

$C_e(^3P_0) = 0$ because the 3P_0 level does not have HFS. From Eq. (3) the nuclear electric-quadrupole moment can be estimated for the three excited xenon levels 3P_2 , 3P_1 , and 1P_1 . The values obtained are

$$^3P_2 \quad Q = -0.12(1) \times 10^{-3} \text{ fm}^2,$$

$$^3P_1 \quad Q = -0.11(1) \times 10^{-3} \text{ fm}^2, \quad (5)$$

$$^1P_1 \quad Q = -0.055(1) \times 10^{-3} \text{ fm}^2.$$

These results confirm the semiempirical analysis of Faust and McDermott [7], which determine the value of Q as $-0.120(15) \times 10^{-3} \text{ fm}^2$ and are also in agreement with more recent measurements of the HFS muonic ^{131}Xe , where $Q = -0.116(4) \times 10^{-3} \text{ fm}^2$ [18]. The consistent displacement observed for the nuclear moment calculated through the 1P_1 level could be ascribed to the influence of the perturbation of $6p$ levels ($2p_{10}$ level is only 84 cm^{-1} above the 1P_1 one) which was not included in the theory.

B. Isotope shift

As is well known, the isotope shift is given by two contributions: mass shift and field shift. As a general rule, for light atoms ($Z < 30$) mass shift is the dominant contribution while for heavy atoms ($Z > 60$) the volume shift plays the main role. For intermediate atoms the two contributions are comparable and, since they can also exhibit different signs, they partially cancel each other. This is the case with xenon ($Z = 54$) for which we observed a rather small IS for all the investigated transitions. In addition, in spite of the high resolution offered by Doppler-free techniques, the large number of isotopes and the rich hyperfine patterns caused a crowded spectra which limited the resolution. This can be easily seen from Fig. 3 where the central part of the spectrum concerning the even isotopes of $1s_4 \rightarrow 2p_5$ [part (a)] and of $1s_5 \rightarrow 2p_6$ [part (b)] transitions are compared. The first transition, as previously discussed, was investigated in a cell where the homogeneous width was about 50 MHz. As can be seen from Fig. 3(a), since the separation between the even isotopes is comparable with the homogeneous width and the

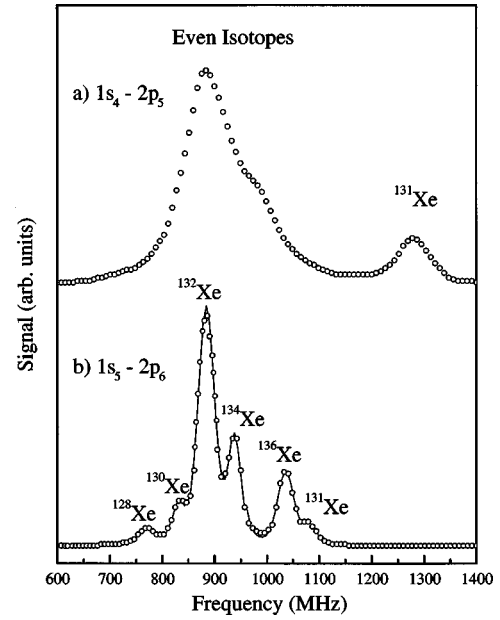


FIG. 3. Doppler-free spectra of the $1s_4 \rightarrow 2p_5$ (a) and $1s_5 \rightarrow 2p_6$ (b) transitions. Both spectra concern only the even isotopes, corresponding to the central part of the spectrum in 2(b). (a) represents the saturated absorption spectrum recorded in the cell while (b) is the fluorescence spectrum obtained on the atomic beam. As explained in the text, only for beam measurement the resolution was enough to allow a reliable fit procedure (continuous line in the lower spectra).

isotope abundance are quite different, the assignment of the isotope centers is also difficult using a fit procedure. On the contrary, the resolution offered by the atomic beam allowed us to assign all the peaks through a fit procedure [continuous line in Fig. 3(b)].

For this reason, among the lines being investigated, it was only possible to completely solve all the xenon isotopes for the $1s_3 \rightarrow 2p_4$ ($\lambda = 820.8 \text{ nm}$) and $1s_5 \rightarrow 2p_6$ ($\lambda = 823.3 \text{ nm}$) lines. The weak peaks of the ^{124}Xe and ^{126}Xe (natural abundance $\approx 0.01\%$) represents an exception because they are completely masked by the larger neighboring isotope peaks. Nevertheless, it is worth noting that rare isotopic species with similar natural abundances were observed by using the same experimental apparatus. This was the case with argon which has two rare isotopes ($^{36}\text{Ar}:0.337\%$ and $^{38}\text{Ar}:0.063\%$) besides the most abundant isotope ^{40}Ar . These, however, are separated by several hundreds of MHz [19]. For odd isotopes, the IS was determined by calculating the position of the center of gravity of the hyperfine multiplet. The IS values for the two above cited transitions are detailed in Table III. As we can see, there is a close agreement with both Doppler-limited conventional spectroscopic data (Ref. [3]) and data gained using a collinear beam laser technique (Ref. [8]), however our measurements increase the accuracy by about one order of magnitude.

Since IS measurements reveal the nuclear shell very distinctly, the structure at magic numbers can cause striking anomalies in the behavior of the IS itself. This is shown in Fig. 4 where the IS values of Table III are plotted against the atomic number A . The shifts between even isotopes are essentially proportional to A except for the couple 136–134 where the $N = 82$ neutron shell is filled.

TABLE III. Isotope shifts of xenon stable isotopes (in MHz). The uncertainties are one standard error obtained over a set of 20 recordings.

Transition	Pair	$\Delta\nu_{\text{expt}}$ (this work)	Other results			$\Delta\nu^0_M$	$\Delta\nu_{\text{SMS}}$ (this work)	$\Delta\nu_F$ (this work)
			Ref. [3]	Ref. [8]				
$1s_5 \rightarrow 2p_6$ (823.3 nm)	136–134	−97.8(8)	−96(9)	−97(3)	21.930	−17(7)	−98(10)	
	136–132	−150.3(4)	−147(9)	−150(4)	44.525	−40(7)	−159(16)	
	136–131	−245(2)	−228(15)	−229(15)	56.080	−51(7)	−244(24)	
	136–130	−202(4)	−201(9)	−203(6)	67.814	−63(7)	−206(21)	
	136–129	−274(2)	−270(15)	−271(7)	79.757	−75(7)	−261(26)	
	136–128	−267.5(4)	−264(9)	−261(10)	91.831	−87(7)	−271(27)	
$1s_3 \rightarrow 2p_4$ (820.8 nm)	136–134	−80.3(8)	−90(6)		21.998	−8(8)	−91(10)	
	136–132	−132.3(3)	−129(5)		44.662	−31(8)	−149(16)	
	136–131	−191(2)	−192(8)		56.253	−42(8)	−228(26)	
	136–130	−183.0(4)	−183(5)		68.023	−54(8)	−228(22)	
	136–129	−238(2)	−234(5)		80.003	−66(8)	−224(28)	
	136–128	−239.8(5)	−243(6)		92.114	−78(8)	−253(30)	

Another interesting phenomenon is so-called “odd-even staggering” which consists in the fact that the center of gravity of the hyperfine splittings of an odd isotope does not lie in midway between the frequency positions of the adjacent even isotopes but is shifted towards the lighter one [20]. This phenomenon is illustrated in Fig. 4 for both the odd isotopes ^{129}Xe and ^{131}Xe since $\Delta\nu^{136-129}$ and $\Delta\nu^{136-131}$ are beneath the straight line passing through the even pairs. For a deeper and more quantitative analysis of the IS it is useful to follow the formalism of Ref. [21]. We can denote the IS for a given transition a between two isotopes α and β with mass number A^α and A^β as the sum of mass shift, $\Delta\nu_M$, and field shift, $\Delta\nu_F$, e.g.,

$$\Delta\nu_a^{\alpha,\beta} = \Delta\nu_M + \Delta\nu_F = \Delta\nu_M^0 K_a + F_a C^{\alpha,\beta}, \quad (6)$$

where $\Delta\nu_M^0$ is the normal mass shift (NMS) and K_a a coef-

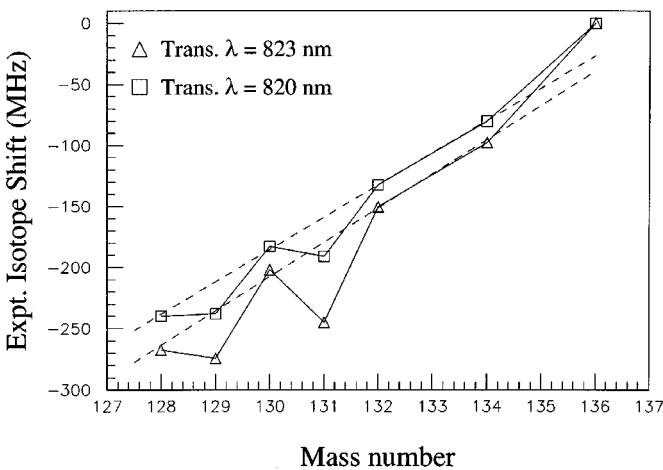


FIG. 4. Behavior of the experimental IS versus the isotope mass number for both $1s_4 \rightarrow 2p_5$ (a) and $1s_5 \rightarrow 2p_6$ (b) transitions. The dashed lines refer to linear fits concerning the even isotopes. The displacement from the straight line of the ^{136}Xe is due to the closed neutron shell of this nucleus while that of ^{129}Xe and ^{131}Xe is ascribed to the odd-even staggering.

ficient which describes the contribution due to the correlation among electrons. The IS related to this effect is named specific mass shift (SMS) and is given by $\Delta\nu_{\text{SMS}} = \Delta\nu_M^0 (K_a - 1)$.

While the calculation of $\Delta\nu_M^0$ simply follows from the mass of the isotopes and the wavelength of the transition, the determination of SMS is much more complicated being K_a dependent on the electronic wave functions of the levels involved in the transition.

Similarly, the field factor F_a appearing in Eq. (7) depends on the wave functions as well and, for an $ns-np$ transition, is given by

$$F_{ns-np} = \frac{\pi a_0^3}{Z} |\Delta\Psi(0)|_{ns-np}^2 f(Z), \quad (7)$$

where a_0 is the Bohr radius, $f(Z)$ is a relativistic correction ($f(54) = 11.37 \text{ GHz/fm}^2$ [22]), and $|\Delta\Psi(0)|_{ns-np}^2$ is the change in the total electron-charge density at the nucleus. As a first approximation $|\Delta\Psi(0)|_{ns-np}^2 = \beta |\Psi(0)|_{ns}^2$ [23], where the screening factor β takes into account the change in the screening of inner closed-shell electrons from the nuclear charge by the valence electron as it changes from ns to np .

Finally, the parameter $C^{\alpha,\beta}$ of Eq. (6) depends on the change in the mean-square nuclear radius for the isotope pair being considered, i.e., $C^{\alpha,\beta} = \delta\langle r^2 \rangle^{\alpha,\beta}$. Nuclear radii are known for a wide variety of nuclei; they vary in a very complicated manner when protons or neutrons are added to the nucleus as discussed in Ref. [24].

In order to obtain physical information on IS it is important to extract the FS and the SMS contribution. King-plots are essentially a basic approach to do that. Indeed, when the IS of two transitions a and b are plotted against each other in an x - y diagram for each isotope pair, the experimental points are distributed around a straight line whose slope is the ratio F_a/F_b , i.e., the ratio of the two field factors of the plotted transitions. In our case, if we plot the $1s_5 \rightarrow 2p_6$ transition along the x axis (denoted as x) and the $1s_3 \rightarrow 2p_4$ transition

(denoted as y) we find $F_y/F_x=0.68(4)$. If the SMS of one transition is known the absolute SMS and FS of the other can easily be calculated. In particular, knowledge of FS allows the estimation of nuclear radii. To the best of our knowledge, there are, in the case of Xe, no data for the SMS or the FS of any transition. For instance, in Ref. [9] the authors assumed a SMS of (56 ± 10) MHz for the 467 nm, line of the 136–134 based on a through review of several empirical methods of determining mass shift (see also Ref. [22] for a wider discussion of this matter).

In order to extract the absolute values of FS and SMS we started from the values of nuclear charge radii available from muonic transitions as reported in Ref. [23]. When the measured IS for a given transition is plotted against $\delta\langle r^2 \rangle^{136,x}$ for all the isotope pairs, a straight line is obtained whose slope is the field factor F while the intercept is the SMS [see Eq. (6)]. The FS and SMS values so calculated for both the transitions are listed in the columns 7 and 8 of Table III. As we can see, the NMS and SMS are of the same order of magnitude and cancel each other meaning that the measured IS must be particularly small. In addition, the ratio between the field factors of the two above cited transitions F_y/F_x is equal to 0.9(1) and is in reasonable agreement with the value 0.68 obtained from the King-plot analysis. It is worth noting that the same result was obtained when different sets of nuclear radii were used as, for instance, the data of Refs. [9], [24], and [25]. This test confirms, in any case, that the assumed mean-square nuclear charge radii are, within the limits of experimental accuracy, consistent with our optical measurements.

The knowledge of the FS allowed us to estimate the screening factor β , the calculation of which is based on Hartree-Fock approaches. The latter are quite difficult especially for non-alkaline-like atoms where configuration mixing occurs and relativistic corrections have to be taken into account. Using the semiempirical Goudsmit-Fermi-Segrè formula (Ref. [22]) and the magnetic dipole constants of the $1s_3$ and $1s_5$ levels reported in Table II we calculated the electronic charge density at the point nucleus of ns electrons:

$$\frac{\pi a_0^3}{Z} |\Psi(0)|_{ns|_{129}}^2 = 0.1553(1);$$

$$\frac{\pi a_0^3}{Z} |\Psi(0)|_{ns|_{131}}^2 = 0.1549(1). \quad (8)$$

Combining these results with Eqs. (2) and (3) we obtained the following screening factors:

$$\beta_{1s_3} = 1.20(5), \quad \beta_{1s_5} = 1.12(4). \quad (9)$$

The only relativistic Hartree-Fock calculation provides a β factor for the $5p^5 6s$ configuration without distinguishing

fine structure [24]; and is equal to 1.16 which is exactly midway between the β factors of the $1s_3$ and $1s_5$ levels.

IV. CONCLUSIONS

In this paper we have performed a high-resolution spectroscopic analysis of the xenon atom in the spectral region of the near-infrared spectral region. Doppler-free spectroscopy was performed either by saturation spectroscopy in cell or by light induced fluorescence spectroscopy on a metastable atomic beam. The latter apparatus gave us a higher resolution but its use was, of course, restricted to transitions starting from the long-lived metastable $1s_5$ level. As a laser source we used a frequency-stabilized semiconductor diode laser.

The HFS and IS of four $1s_J \rightarrow 2p_{J'}$ transitions were investigated in natural samples for all the stable xenon isotopes except ^{124}Xe and ^{126}Xe , which were not naturally abundant enough for the resolution of our apparatus.

For all the levels of the investigated transition the HFS pattern of the two odd isotopes (^{129}Xe and ^{131}Xe) was assigned with an appropriate fitting procedure and the relative magnetic dipole and electric quadrupole HFS constants were estimated. The accuracy of our measurements varied between 0.5% and 7%. For the metastable $1s_5$ level we found a rather close agreement with very accurate NMR measurements, while for most of the remaining levels studied the only available data in the relevant literature were based on Doppler-limited conventional spectroscopy.

The IS investigation was, on the other hand, limited to only two transitions, the $1s_5 \rightarrow 2p_6$ and $1s_3 \rightarrow 2p_4$ lines for which all the even isotopes were fully resolved. Our IS measurements evidenced the simultaneous presence of two well-known phenomena: the first concerns the anomalous behavior of the magic nucleus ^{136}Xe ($N=82$) while the second is the odd-even staggering observed in the correspondence of the two odd isotopes.

In order to extract the two main contributions to the IS, the specific mass shift and the field shift, we started from the muonic nuclear radii (Ref. [23]). As expected, the IS in such a relatively large nucleus as xenon was dominated by field shift. From this analysis we estimated the field factor ratio of the two transitions and found a close agreement with the value calculated from a full optical analysis based on King-plots.

Finally, the screening factors β of the two transitions were calculated using the Goudsmit-Fermi-Segrè formula with the HFS measurements. The values found for the $1s_5 \rightarrow 2p_6$ and $1s_3 \rightarrow 2p_4$ transitions were in agreement with the only theoretical data for the $5p^5 6s$ electronic configuration.

Our results will hopefully stimulate a deeper theoretical analysis of the SMS and FS of xenon. Indeed, such calculation, requiring accurate knowledge of electronic wave function, could provide more accurate and complete information about the nuclear parameters of such an atom.

- [1] D. A. Jackson, F. R. S., M.-C. Coulombe, and J. Bauche, Proc. R. Soc. London, Ser. A **338**, 277 (1974).
 [2] D. A. Jackson, F. R. S., and M.-C. Coulombe, Proc. R. Soc. London, Ser. A **343**, 453 (1974).
 [3] D. A. Jackson, F. R. S., M.-C. Coulombe, and J. Bauche,

- Proc. R. Soc. London, Ser. A **343**, 443 (1975).
 [4] D. A. Jackson, F. R. S., and M.-C. Coulombe, Proc. R. Soc. London, Ser. A **327**, 137 (1974).
 [5] D. A. Jackson, F. R. S., and M.-C. Coulombe, Proc. R. Soc. London, Ser. A **335**, 127 (1974).

- [6] W. Fischer, H. Huhnermann, G. Kromer, and H. J. Schafer, *Z. Phys.* **270**, 113 (1974).
- [7] W. L. Faust and M. N. McDermott, *Phys. Rev.* **123**, 198 (1961).
- [8] W. Borchers, E. Arnold, W. Neu, R. Neugart, K. Wendt, and G. Ulm, *Phys. Lett. B* **216**, 7 (1989).
- [9] H. Geisen, T. Krumpelmann, D. Neuschafer, and Ch. Ottingen, *Phys. Lett. A* **130**, 299 (1988).
- [10] M. D. Plimmer, P. E. G. Baird, C. J. Foot, D. N. Stacey, J. B. Swan, and G. K. Woodgate, *J. Phys. B* **22**, L241 (1989).
- [11] M. Walhout, H. J. L. Megens, A. Witte, and S. L. Rolston, *Phys. Rev. A* **48**, R879 (1993).
- [12] N. Beverini, G. L. Genovesi, and F. Strumia, *Nuovo Cimento D* **17**, 515 (1995).
- [13] C. Wieman and L. Hollberg, *Rev. Sci. Instrum.* **62**, 1 (1991).
- [14] A. A. Radzig and B. M. Smirnov, in *Reference Data on Atoms, Molecules, and Ions*, Springer Series in Chemical Physics Vol. 31 (Springer, Berlin, 1980).
- [15] H. Fabrikant, O. B. Shpenik, A. V. Snegursky, and A. N. Zavilopulo, *Phys. Rep.* **159**, 1 (1988).
- [16] A. Sasso, M. Inguscio, G. Tino, and N. Beverini, *Nuovo Cimento D* **10**, 941 (1988); P. Cangiano, M. de Angelis, G. Pesce, and A. Sasso, *Phys. Rev. A* **50**, 1082 (1994).
- [17] H. Kopfermann, *Nuclear Moments* (Academic, New York, 1958).
- [18] C. M. Lederer and V. S. Shirley, *Table of Isotopes*, 7th ed. (Wiley, New York, 1978).
- [19] G. Pesce and A. Sasso, *Opt. Commun.* **148**, 272 (1997). G. D'Amico, G. Pesce, and A. Sasso, *J. Opt. Soc. Am. B* **16**, 1033 (1999).
- [20] P. Aufmuth and M. Hauer, *Physica B & C* **123C**, 109 (1983).
- [21] J. Bauche and R.-J. Champeau, *Adv. At. Mol. Phys.* **37**, 39 (1976).
- [22] W. H. King, *Isotope Shifts in Atomic Spectra* (Plenum, New York, 1984).
- [23] P. Aufmuth, K. Heilig, and A. Steudel, *At. Data Nucl. Data Tables* **37**, 455 (1987).
- [24] G. Fricke, C. Bernhardt, K. Heilig, L. A. Schaller, L. Schellenberg, E. B. Shera, and C. W. De Jager, *At. Data Nucl. Data Tables* **60**, 177 (1995).
- [25] K. Heilig and A. Steudel, *At. Data Nucl. Data Tables* **14**, 613 (1974).